Chapter 3

Evaluation of W-CMP performance with varying DI water dilution and hydrogen peroxide concentration

3.1 Introduction

In this experiment (table 3-1, table 3-2), I would like to dilute CABOT W2000 (acidic SiO2 suspension, pH=2-3) slurry with 1 to 6 parts of DI water without degradation of polishing performance, removal rate and non-uniformity. Both slurry pH and solid content would be changed during dilution, which dramatically change the abrasive suspension and mechanical abrasion during polishing. Varying hydrogen peroxide concentration of slurry would lead to complicated surface oxidation on W surface, both thermodynamically and kinetically. Not only removal rate would be changed with various oxidizer concentration, the surface oxide passivation also be changed. Dishing of W plugs after polishing would occur during oxide buffing or post CMP cleaning with alkaline solution or dilute HF solution.

In this study, both dilution of CABOT W2000 slurry and various hydrogen peroxide concentration of slurry formulation would be explored for optimized polishing performance, removal rates, non-uniformity and dishing effect.

Mechanical abrasion would be reduced as dilute ratio increase owing to solid content drop, so as to removal rate would be reduced. The removal rates would not significantly changed as dilute ratio up to 4 [1]. It maybe the surface oxide passivation should be varied as dilution. As shown in Pourbaix (fig3-1) [2], tungsten oxide would be more corroded in alkaline sol'n. The pH of W2000 slurry without dilution would be 2-3, but may be changed to 4-6 as dilution. The surface passivation could be evaluated by electrochemical measurement (Tafel & impedance). The other factor may be taken into account is abrasive suspension; aggregation of abrasive may occur during dilution, it may lead to enhance removal rates. Both size analysis and surface roughness being polished by AFM could be implemented for characterization of abrasive effects.

3.2 Experimental

3.2.1 Size and zeta potential measurement

Zetasizer Nano series was used to measure the zeta potential and particle size. The zetasizer Nano series performed size measurements using a process called Dynamic Light Scattering (DLS). Dynamic Light Scattering (also known as PCS-Photon Correlation Spectroscopy) measured Brownian motion and related this to the size of the particle. It did this by illuminating the particles with a laser and analyzing the intensity fluctuations in the scattered light.

A small particle was illuminated by a light source such as a laser, the particle would scatter the light in all directions. A screen was held close to the particle, the screen will be illuminated by the scattered light. Then consider replacing the single particle with thousands of stationary particles. The screen would show a speckle pattern as below.

The diagram showed the propagated waves from the light scattered by the particles. The bright areas of light were where the light scattered by the particles arrived at the screen with the same phases and interferes constructively to form a bright patch. The dark areas were where the phase additions were mutually destructive and canceled each other out. In this situation the speckle pattern would also be stationary – in terms of both speckle position and speckle size. In practice, particles suspended in a liquid were never stationary. The particles were constantly moving due to Brownian motion. Brownian motion is the movement of particles due to the random collision with the molecules of the liquid that surrounds the particle. An important feature of Brownian motion for DLS is that small particles moved quickly and large particles moved more slowly. The relationship between the size of a particle and its speed due to Brownian motion was defined in the Stokes-Einstein equation. As the particles were constantly in motion the speckle pattern would also appear to move. As the particles moved around, the constructive and destructive phase addition of the

scattered light would cause the bright and dark areas to grow and diminished in intensity – or to put it another way, the intensity appeared to fluctuate. The Zetasizer Nano system measureed the rate of the intensity fluctuation and then used this to calculate the size of the particles.

3.2.2 Tafel & EIS (electrochemical impedance spectrocope) Measurement

The special designed apparatus based on the traditional three electrode rotating-disk configuration for in situ CMP measurement is schematically shown in Fig.3-2. The electrochemical cell consisted of a metal cylinder as the rotating working electrode and a Pt mesh net and an Hg/HgSO4 half-cell electrode as the counter and reference electrodes, respectively. The three-electrode electrochemical cell was connected to an EG&G lock-in amplifier model 5301 and potentiostat model 273, and immersed in the slurry with a Rodel Politex regular E polishing pad at the bottom. The working electrodes were made of a W ~99.99% Cylinder embedded in epoxy resin (1 cm2); only one side of the cylinder was exposed to the slurry.

For EIS measurements, the polishing condition was fixed at a 45 rpm rotational speed and 4 psi downward pressure, the amplitude of the perturbation was ±10 mV, and the frequency varying from 0.1 Hz to 100 kHz at 6 steps/dec. The slurry used in the experiments contained 0.5 M citric acid and 5 vol % phosphoric acid as the pH

buffer solution, 0.05 mm Al2O3 abrasive particles of 5 wt %, and 0-10 vol % H2O2 as the main oxidizer. The slurry pH was adjusted from 2 to 6 by adding KOH. Z view version 2.1a computer software was used for the curve fitting and analysis of the impedance.

Polishing experiments were carried out on a Westech 372M polisher with a Rodel Politex regular E polishing pad and Rodel R200-T3 carrier film. For the Al polishing process, the polishing parameters of pressure, platen and carrier rotary speeds, back pressure, and slurry flow rate were set to 4 psi, 60 and 65 rpm, 2 psi, and 150 mL/min, respectively. In the Ti polishing step, back pressure and slurry flow rate were the same as the Al polishing process, with platen and carrier rotary speeds adjusted to 45 and 42 rpm, respectively.

3.2.3 CMP Process

Polisher Setup

A Westech Model 372M CMP processor (Figure 2-1.), consisting of a wafer carrier and a primary circular polishing table mounted with Rodel IC 1400^{TM} grooved (made of polyurethane impregnated polyester) pad and a secondary buffing table mounted with an Rodel Politex Regular E.^{TM} pad, a carrier to hold wafers against the pad, and a Rodel R200-T3 carrier film to provide buff between the carrier and wafer was used for CMP experiments. Recesses in the carrier template mechanically constrain a

single 6-inch wafer, preventing it from sliding out from under the carrier during polishing. A polymeric film placed in the recess brought the wafer slightly above the surrounding template surface. When the film was wetted, it provided sufficient surface tension to hold the wafer while it is being positioned over the polishing table. The teflon retaining ring was recessed from the wafer surface about 7 miles. The slurry, pumped out from a reservoir at a controlled rate, was dispensed onto the center of the table. The table and the carrier were both motor driven spindles, rotated independently at constant angular velocities (rpm). The arm was oscillated about their position at half radius of the table to utilize more pad area and to reduce pad wear. Pressure at the wafer-slurry-pad interface was controlled via an overhead mechanism, which allowed pressure to be applied onto the wafer carrier.

Pad Prewet & Pad Conditioning

Pad prewet was performed before the start of each polishing action. The prewet slurry flow rate was at 300 ml/min and the prewet time was fixed at 20 seconds. Pad conditioning was employed to resurface the pad in order to maintain the removal rate without sacrificing uniformity. The purpose of pad conditioning was to clean the slurry residuals and to lift the pad fiber for further processing. Without this procedure, the polishing rate decreased substantially after several polishing cycles. In our

experiments, pad conditioning was done by brush artificially. Pad conditioning was performed before and between each wafer, and polishing was terminated before pad glazing could cause significant reduction in removal rate.

Polishing Recipes & Slurry Formations

The polishing recipes and slurry formulations in cleaning experiment were all listed in the Table.. The commercial W2000 slurry was fumed silica abrasives with the size of 30-50 nm approximately. The other slurry were consisted of organic acids ‘DIW and Al2O3 abrasive. In the phase1, oxide layers were polished to establish the fresher surface and would bond with tungsten or copper ions easily. Phase2 is to remove the residual slurry from wafer surface.

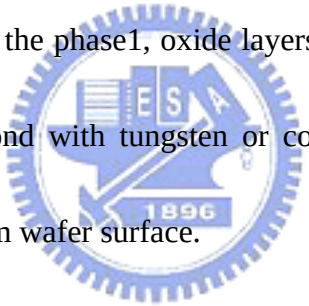

3.2.4 ESCA Analysis

ESCA was based on the photoelectric effect. When a solid was exposed to a flux of X-ray photos of known energy, photoelectrons were emitted from the solid. This photoelectron was emitted with a kinetic energy characteristic of the difference between the X-ray and binding energy of the electron. The energy of the emitted photoelectron defines the type of atom, and the number of photoelectrons at this energy was related to the number density of atoms present. A schematic drawing of a typical ESCA spectrometer was show in Figure.3-3 [20]. ESCA analysis was

performed on Americould Physical Electronics ESCA PHI 1600 with Al anode (1486.6 eV).

In this study, electron spectroscopy for chemical analysis (ESCA) was employed to analysis the existence of WO_3. WO_3 has C、W、N atoms, but C atoms polluted wafers easily from air or hand-touch contamination. Hence, we observed N atoms to distinguish if BTA coordinate with Cu^+ ion on the Cu surface.

3.3 Results and Discussions

3.3.1 Zeta potential and abrasive size

The zeta potential and abrasive size were measured by Zetasizer Nano. Each of the zeta and size was measured six times to compile statistics that was shown in Figure 3-4, 3-5, 3-6, 3-7.

In part 1, it was obvious that while the dilution ratio increased, the abrasive size became small. While dilution ratio increased the solution changed the chemical composition. It would affect the electrostatic double layer reduce the secondary particle size. Zeta potential was not strongly significant and dense because that was not larger than 30mv or smaller than -30mv. The titrations of the raw slurry and the other dilution ratio could be understand the pH near the IEP (iso-electrical point). The raw slurry and the other dilution ratio would easily to precipitate. Each of titration

shown in the Figure 3-8 ~ 3-14. While dilution ratio of titration increased, the size become smaller.

In part 2, it was obvious that with hydrogen peroxide was apparently different from that without hydrogen peroxide. The hydrogen peroxide content would not a key point for the abrasive size. The zeta potential also was so small that easily to precipitate.

3.3.2 Electrochemical results

In the solution, water and ions typically diffused into an organic coating, after a coated metal was submerged in an electrolyte, and change coating dielectric properties. Water and ions also moved inside a coating in response to AC polarizations. Water and ions movement through a coating was restricted by coating morphology, or pore resistance. Coating time constants could change with time, as electrolyte concentration in the coating changes. A corroding coated metal surface: a two time constant system (figure 3-15). Small minus signs in figure 3-15 represent negative ions, positive signs represent positive ions, and the others were electrochemically active species and water molecule. Nested circuits were used, instead of circuits in series, to indicate that pores in a coating could cause metallic corrosion by providing areas where the electrolyte had direct access to the metal surface. Tafel and EIS results shown in the figure 3-16 ~ 3-19. In the tafel (part 1),

we can observed while the 2% hydrogen peroxide added the ocp (open circuit potential) shift to about 0.4v. While the dilution ratio increased, the ocp slightly increased. Although the ocp of dilution ratio differ from each other, the corrosion current would not change a lot. It meant that the corrosion rate for the tungsten would almost be the same. In the EIS (part 1), while the dilution ratio increased, the solution resistance (Rs) become larger. The complicated impedance of EDL and passivation layer with 2% hydrogen peroxide almost become the single EDL impedance. It meant that the tungsten immersed into the solution would not produce the passivation layer. The mechanism of the CMP almost the chemical etching dominated, that shown in figure 3-34 & 3-35, that polishing rate would not change violently to fit in with the electrochemical results. There was a significant result in the Tafel (part2), while the hydrogen peroxide added. The ocp changed about 0.3v (figure 3-18) and the anodic branch without hydrogen peroxide become more vertical. It could be match the EIS (figure 3-19). The more vertical line in the Tafel, the lager circle in the EIS and the solution resistance won't change very violently. In order to match the tungsten-H2o pourdaix diagram (figure 3-1) that produce the passivation layer , we changed the pH under pH=2 and measured the Tafel and EIS in the figure 3-20 ~ 3-23. However, the Tafel and EIS results would not match the tungsten-H2O pourdaix diagram. We explained that W2000 would not similar to the DIW. W2000 contained some

unknown chemical composition that could make tungsten surface corrosive.

3.3.3 Electrical evaluation

In this step, we known if the hydrogen peroxide were added that the mechanism of CMP were dominated by etching. We could make via chain structure to verify it. Via chain structure shown in figure 3-36 & 3-37. Then, we measured it with 300 tungsten plugs totally 5 sites and the results would be normalized that shown in table 3-5 & 3-6. While hydrogen peroxide was added the resistance would become smaller than the other. The results would conform to electrochemical results.

3.4 Summary

In this study, the dilution ratio increased that the abrasive would lead to smaller, polishing rate to conform to the result of using Zetasizer Nano , shown in figure 3-5 & figure 3-34, but the polishing rate degree still could be accepted. In the other experiment, the polishing rate also conform to the data of using Zetasizer Nano, shown in figure 3-6 & figure 3-35. While the dilution ratio increased, the corrosion current would decrease, shown in table 3-7, that also conformed to polishing rate, shown in figure3-34. The other result, shown in table 3-9, also conformed to the other polishing rate, shown in figure 3-35. It obvious to understand while the hydrogen peroxide added in the slurry, that the corrosion current would become larger and the surface oxide (Rcoat) become to zero, shown in table 3-8 ~ table 3-10, so we could

define the polishing rate almost dominated by etching. The particle size became larger or smaller that just a little effect could affect the polishing rate. Then, the data of esca , shown in figure 3-30 ~ figure 3-33, could explain that surface oxide (WO3) formed by the composition without hydrogen peroxide similar to the data of slurry with hydrogen peroxide. It meant that the composition without hydrogen peroxide would not form thick surface oxide than the composition with hydrogen peroxide. Two surface oxides nearly formed by the native oxide. Lastly we made via chain structure to prove while surface oxide became thicker, that contact resistance would become larger, shown in table 3-5 and table 3-6.

Table 3-1 Part I: Dilute ratio with 1-6 parts of DI water

NO	**Dilute ratio (slurry : DI water)**	H2O2
1	1:1	2%
2	1:2	2%
3	1:3	2%
4	1:4	2%
5	1:5	2%
6	1:6	2%

Table 3-2 Part II: Concentration of hydrogen peroxide

	Dilution ratio	H2O2
1	1:3	0
2	1:3	1%
3	1:3	2%
4	1:3	2.5%
5	1:3	3%
6	1:3	3.5%
7	1:3	4%
8	1:3	6%
9	1:3	8%
10	1:3	10%

Table 3-3 Content distribution of experimental part1

	W2000	DIW	H2O2	Total volume	pH
Raw					2.02
1:1	50	43.5	6.45	100	2.18
1:2	33.33	60.25	6.45	100	2.22
1:3	25	68.55	6.45	100	2.28
1:4	20	73.55	6.45	100	2.33
1:5	16.67	76.88	6.45	100	2.36
1:6	14.285	79.26	6.45	100	2.41

Table 3-4 Content distribustion of experimental part2

	W2K	H2O2(mL)	Total vol (mL)	pH
0%	25	0	100	2.46
1%	25	3.25	100	2.41
2%	25	6.45	100	2.35
2.5%	25	8.06	100	2.41
3%	25	9.68	100	2.4
3.5%	25	11.3	100	2.48
4%	25	12.9	100	2.41
6%	25	19.35	100	2.4
8%	25	25.8	100	2.25
10%	25	32.26	100	2.22

Table 3-5 Electrical evaluation without H2O2

	Site1	Site2	Site3	Site4	Site5	Avg(Ω)
1:1,0%	4.0	4.2	4.0	4.1	4.3	4.12
1:3,0%	4.0	4.1	3.9	4.0	4.2	4.04

Table 3-6 Electrical evaluation with H2O2

	Site1	Site2	Site3	Site4	Site5	Avg(Ω)
1:1,2%	3.7	3.7	3.7	3.6	3.7	3.68
1:3,2%	3.5	3.6	3.7	3.6	3.7	3.62

Table 3-7 Corrosion current of Tafel plot in experimental part1

	H2O2	Corrosion Current (1E-4A/cm2)
Raw		0.525
01:01	2%	1.35
01:02	2%	0.973
01:03	2%	0.966
01:04	2%	0.724
01:05	2%	0.617
01:06	2%	0.589

Table 3-8 EIS equivalent circuit in experimental part1

	Raw	01:01	01:02	01:03	01:04	01:05	01:06
H2O2		2%	2%	2%	2%	2%	2%
Rs (Ω)	179	346	465	586	722	797	929
Ccoat (F)	0.0001	0.007	0.007	0.007	0.007	0.007	0.007
Rcoat (Ω)	650	0	0	0	0	0	0
Cdl (F)	0.05	0.006	0.006	0.006	0.006	0.006	0.006
Rdl (Ω)	170	85	85	85	85	85	85

Table 3-9 Corrosion current of Tafel plot in experimental part2

	Corrosion Current (1E-4A/cm2)
0%	0.299
1%	0.797
2%	0.893
2.5%	0.979
3%	0.793
3.5%	0.719
4%	0.859
6%	1
8%	0.841
10%	1.07

Table 3-10 EIS equivalent circuit in experimental part2

H_2O_2	0%	1%	2%	2.5%	3%	3.5%	4%	6%	8%	10%
Rs (Ω)	543	550	580	770	543	543	645	655	543	543
Ccoat (F)	0.005	0.007	0.007	0.007	0.007	0.007	0.007	0.007	0.007	0.007
Rcoat (Ω)	950	0	0	0	0	0	0	0	0	0
Cdl (F)	0.05	0.006	0.006	0.006	0.006	0.006	0.006	0.006	0.006	0.006
Rdl (Ω)	175	165	95	95	75	70	60	50	30	20

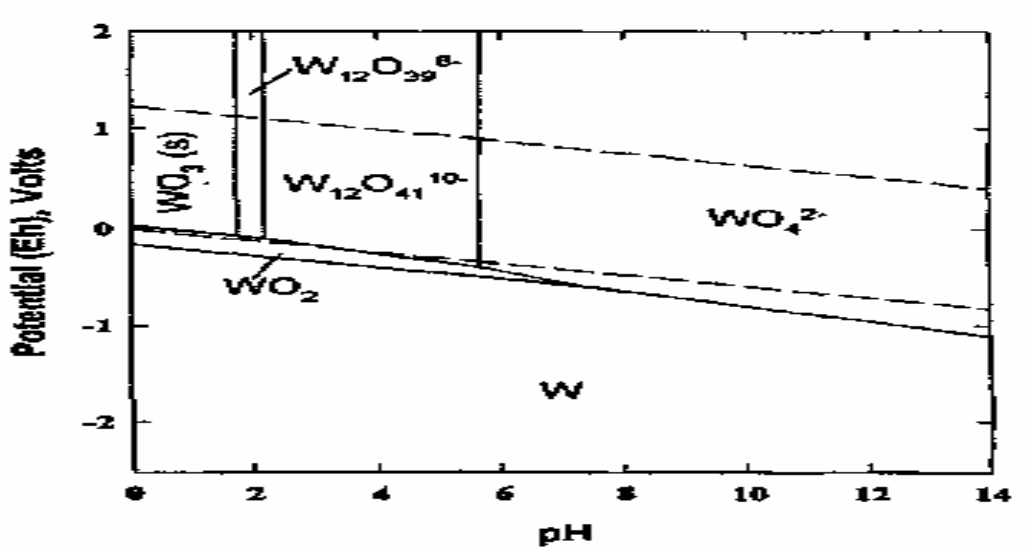

Figure 3-1 W-H2O pourbaix diagram

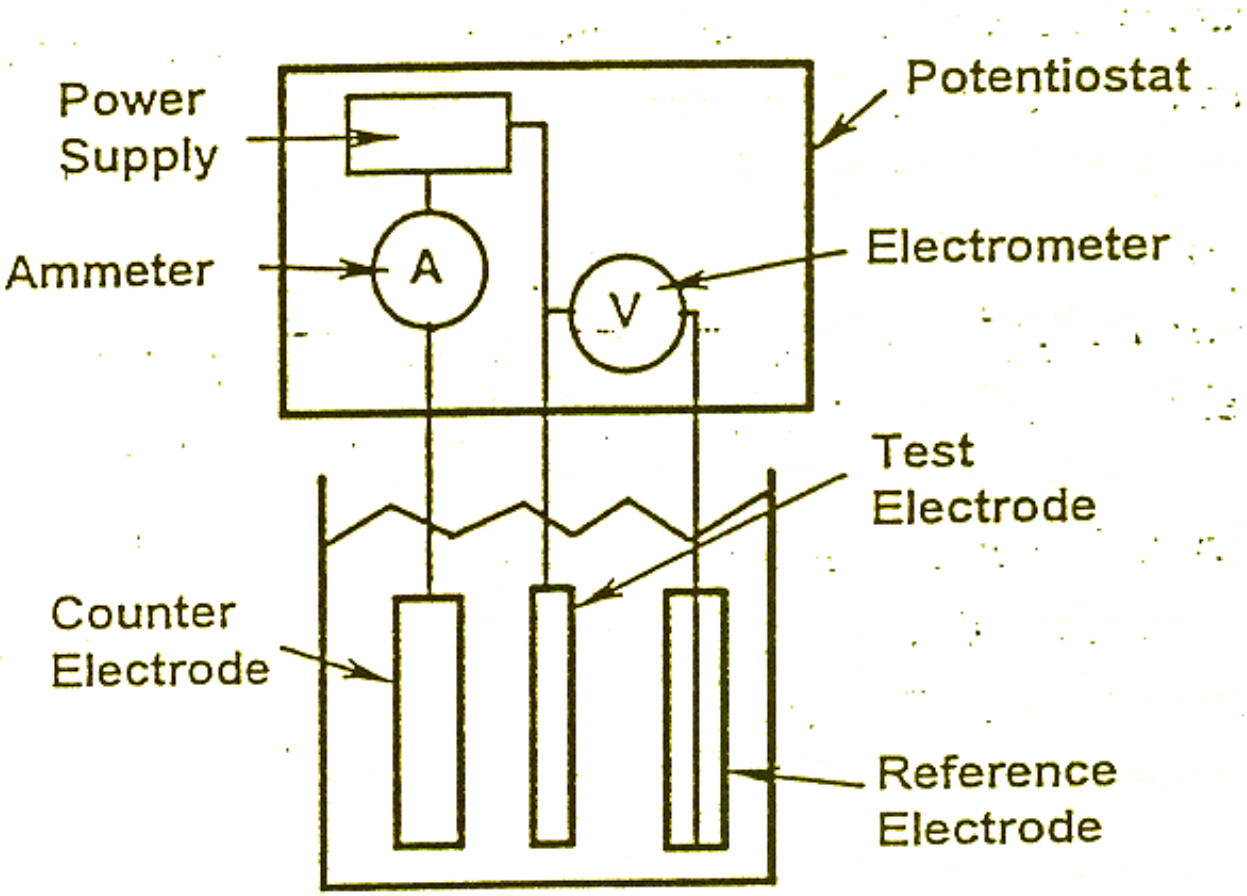

Figure 3-2 Three electrode test cell schematic.

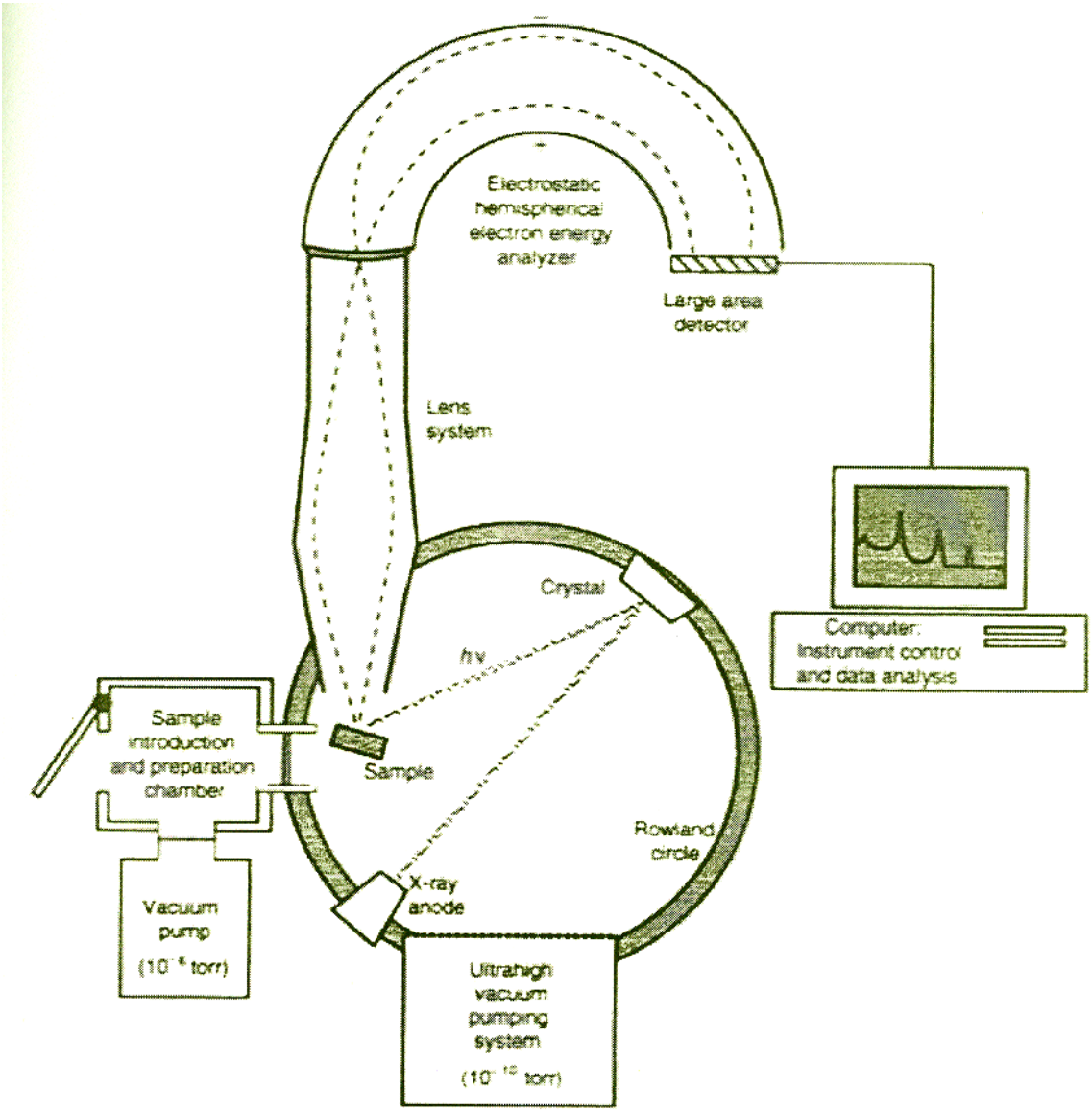

Figure 3-3 A schematic diagram of an ESCA spectrometer.

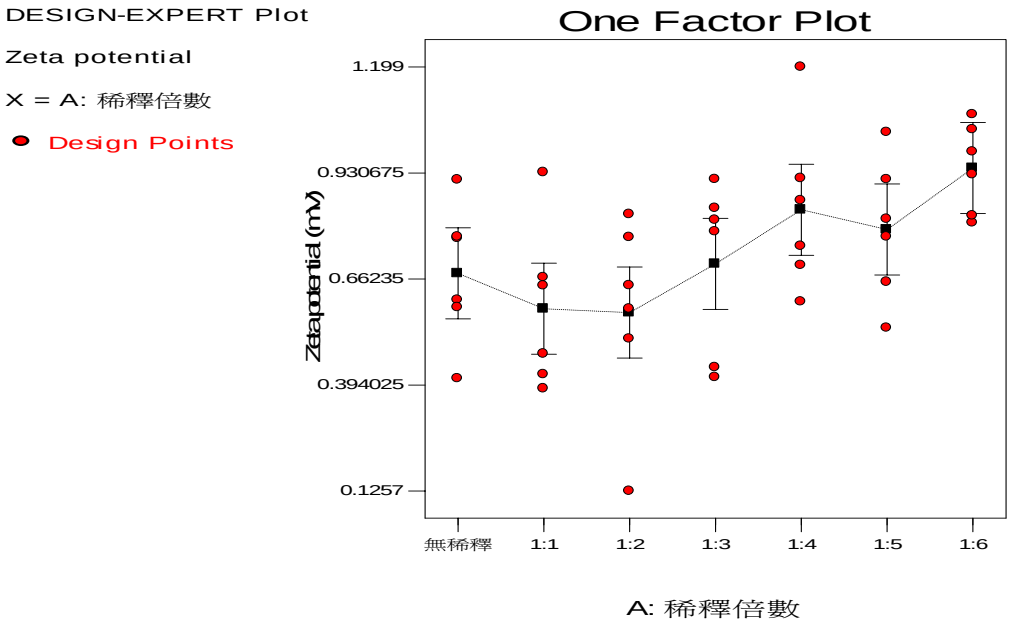

Figure 3-4 Zeta potential of experimental part1

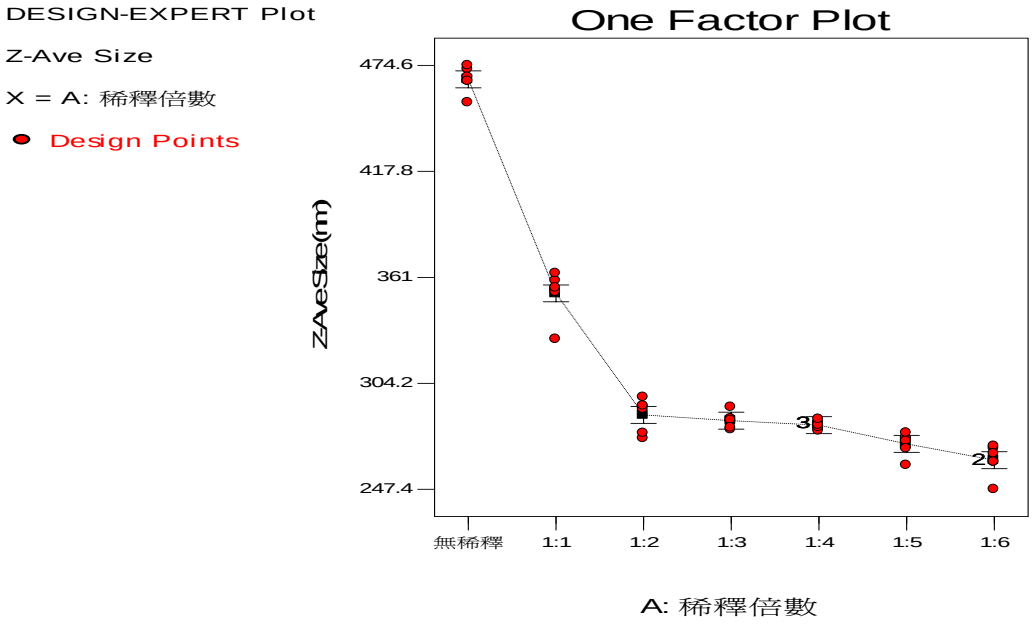

Figure 3-5 Particle size of experimental part1

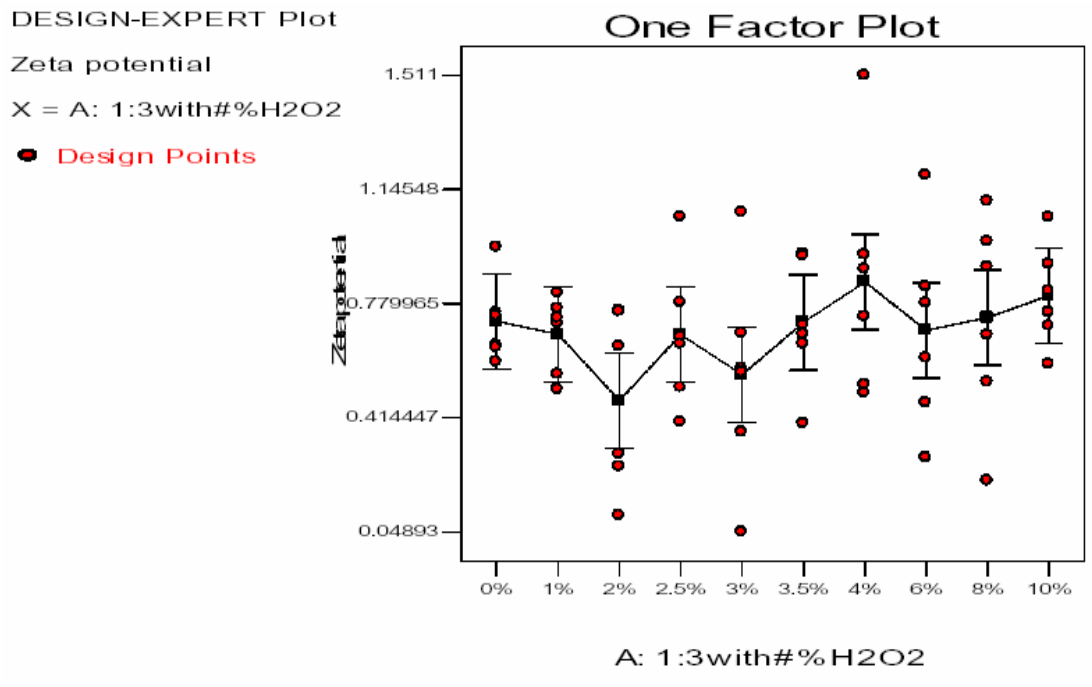

Figure 3-6 Zeta potential of experimental part2

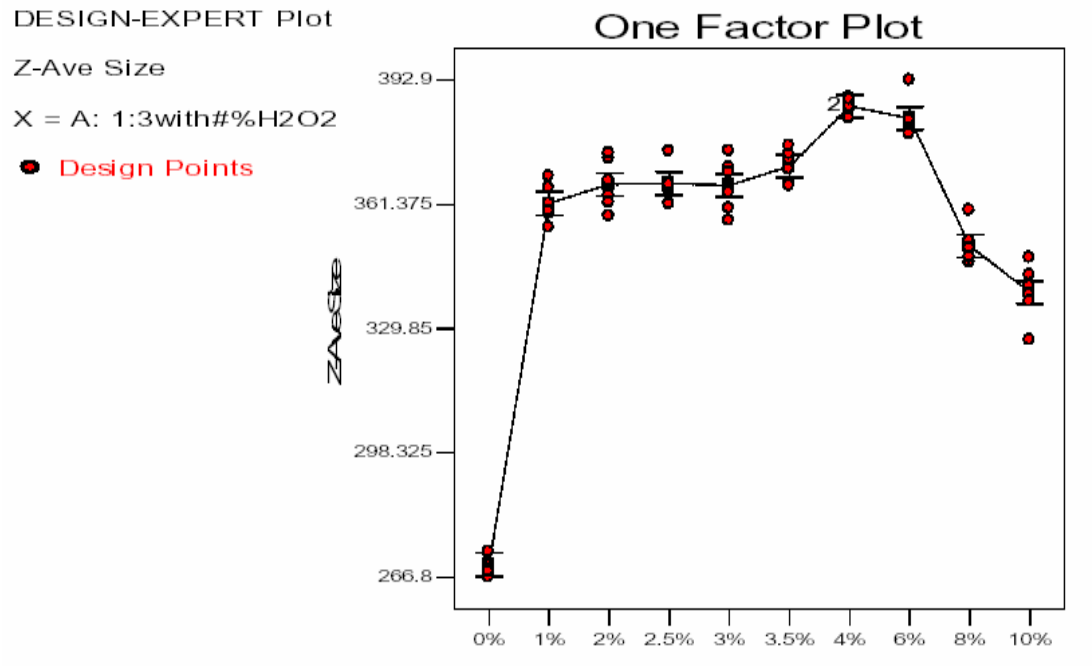

Figure 3-7 Particle size of experimental part2

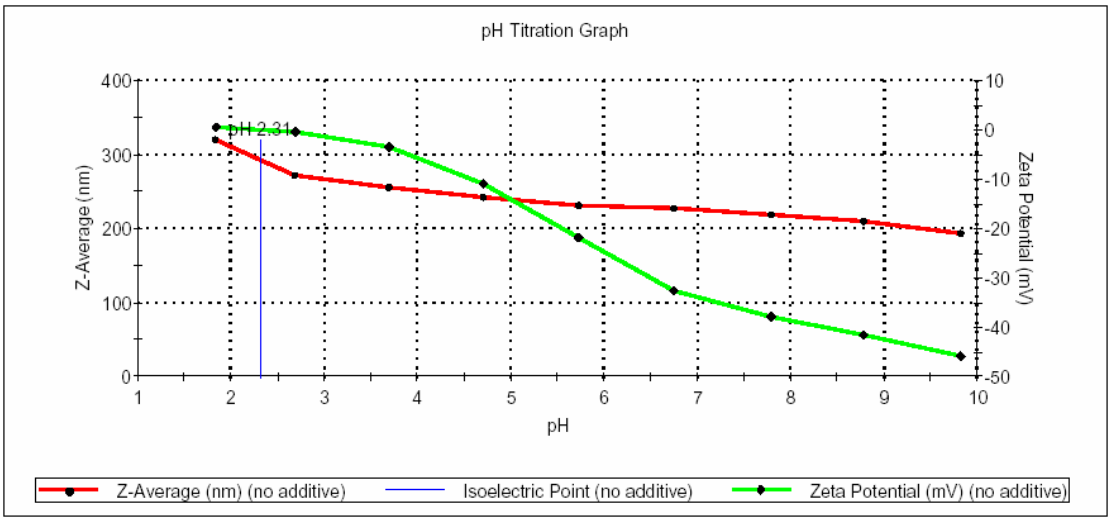

Figure 3-8 Titration of Raw

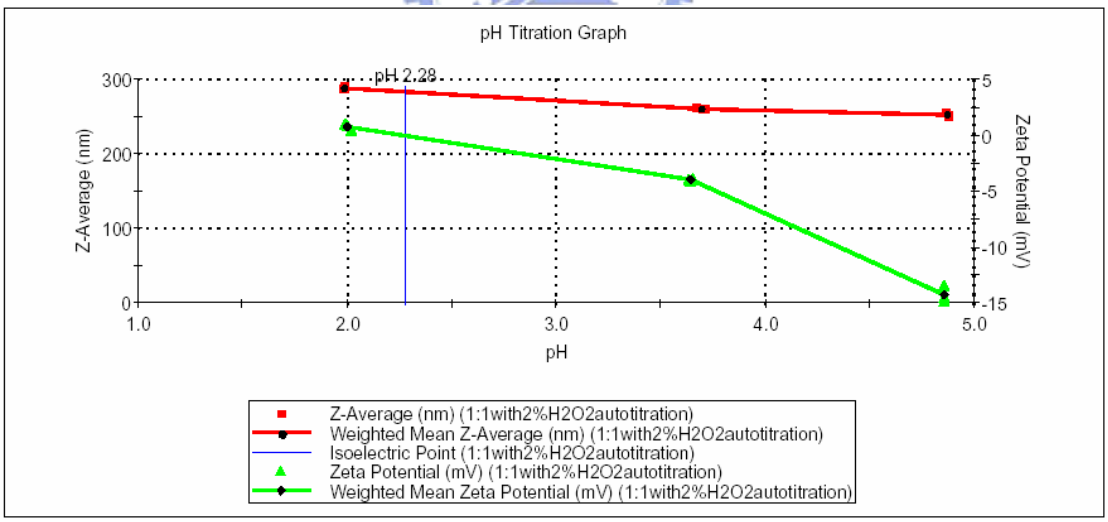

Figure 3-9 Titration of 1:1 with2%H2O2

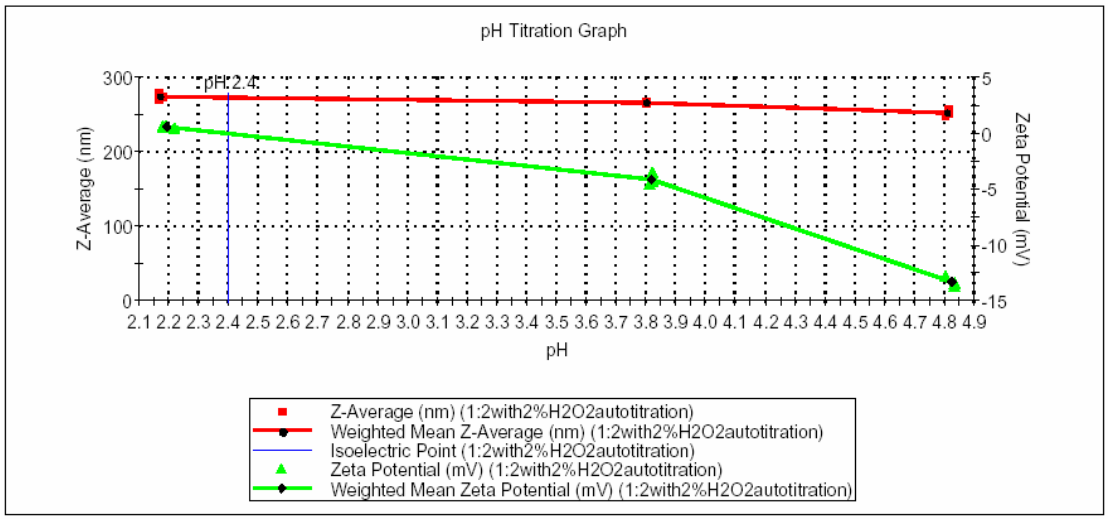

Figure 3-10 Titration of 1:2 with2%H2O2

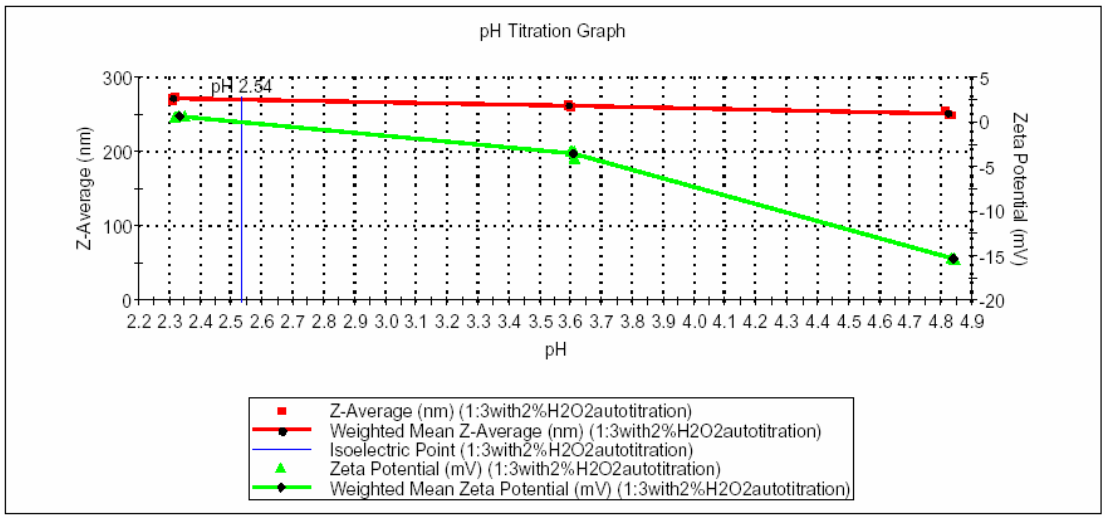

Figure 3-11 Titration of 1:3 with2%H2O2

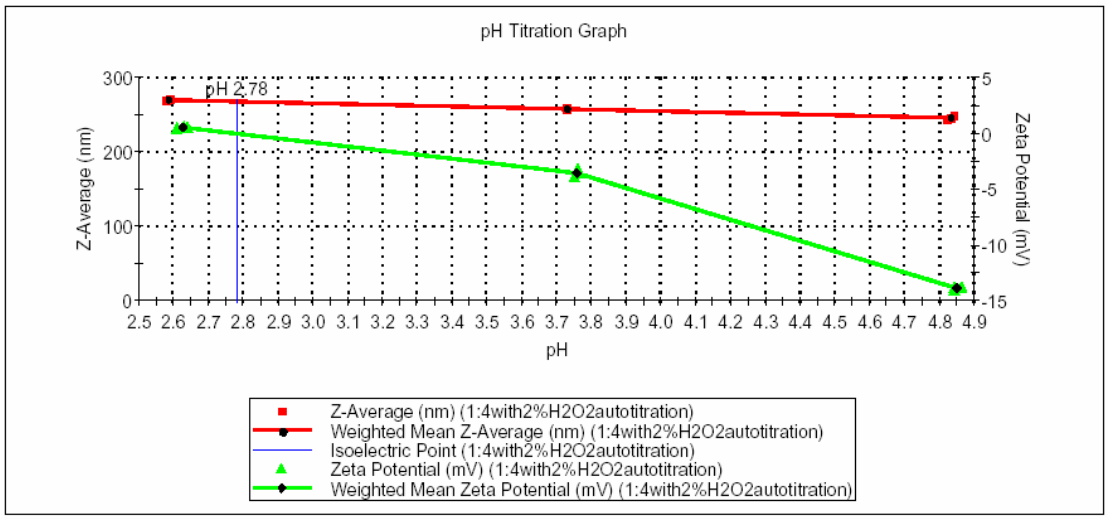

Figure 3-12 Titration of 1:4 with2%H2O2

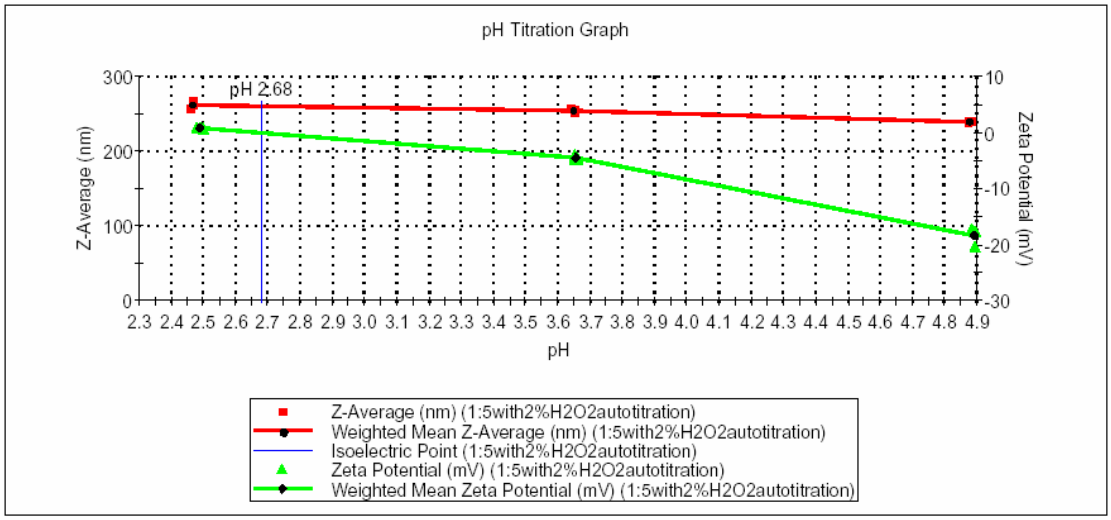

Figure 3-13 Titration of 1:5 with2%H2O2

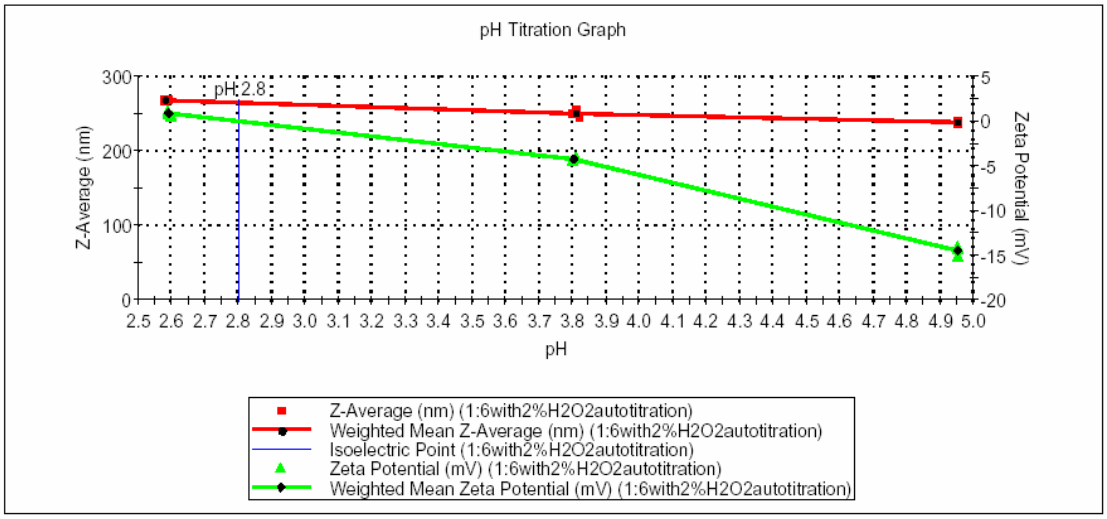

Figure 3-14 Titration of 1:6 with2%H2O2

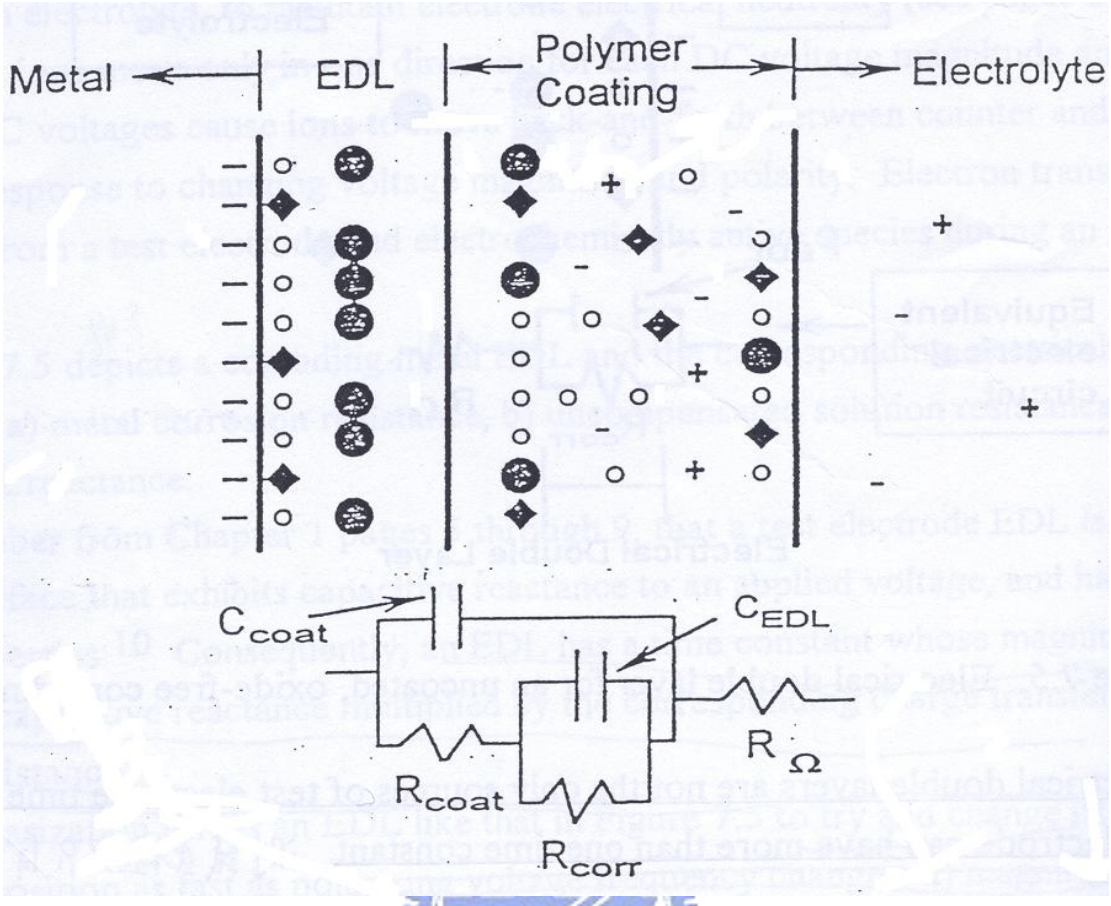

Figure 3-15 Equivalent circuit of EDL and surface coating

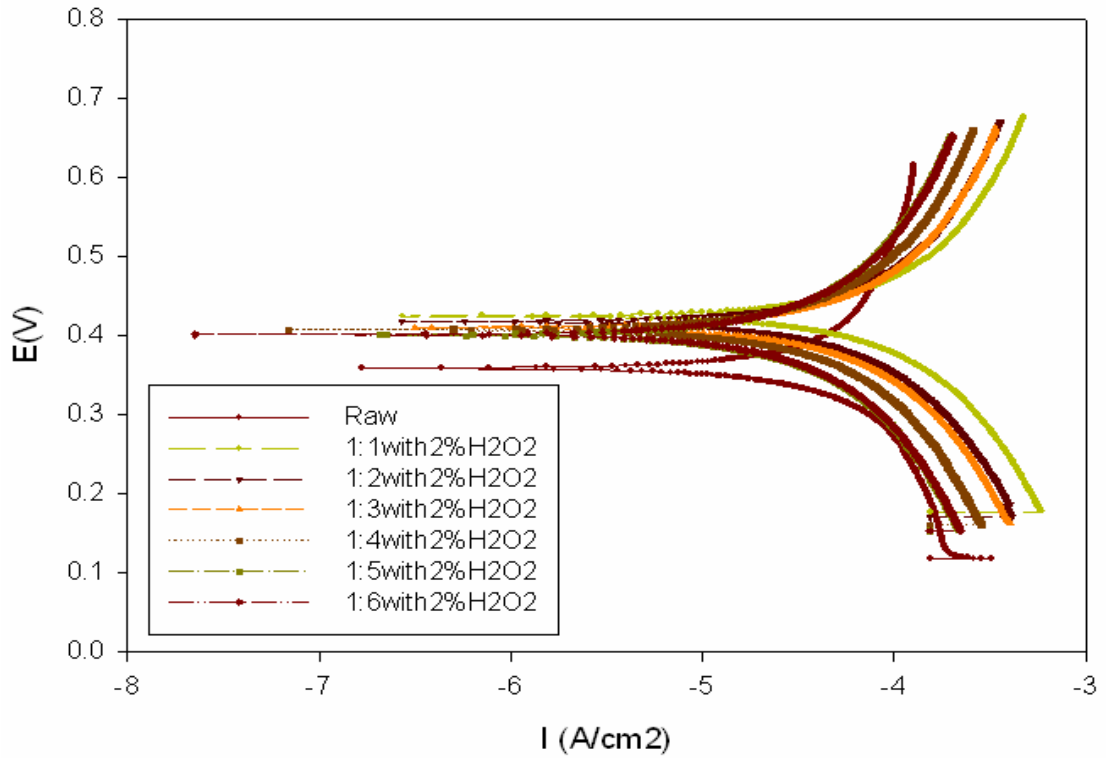

Figure 3-16 Tafel of experimental part1

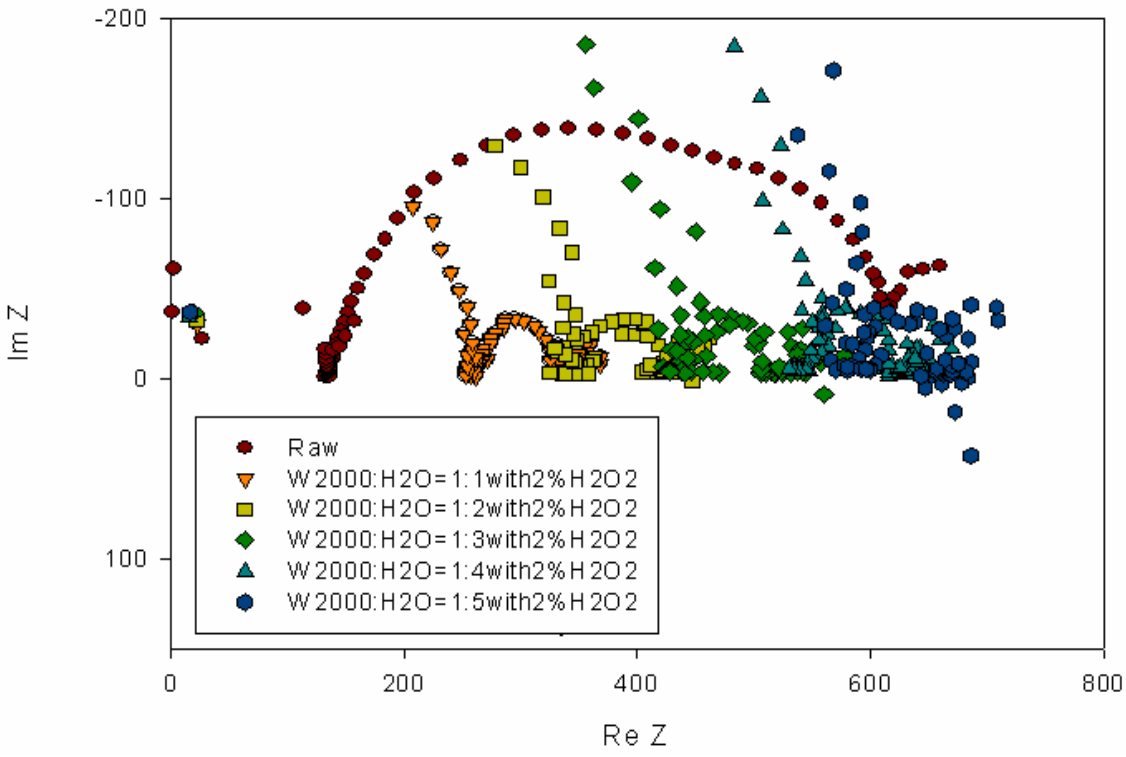

Figure 3-17 EIS of experimental part1

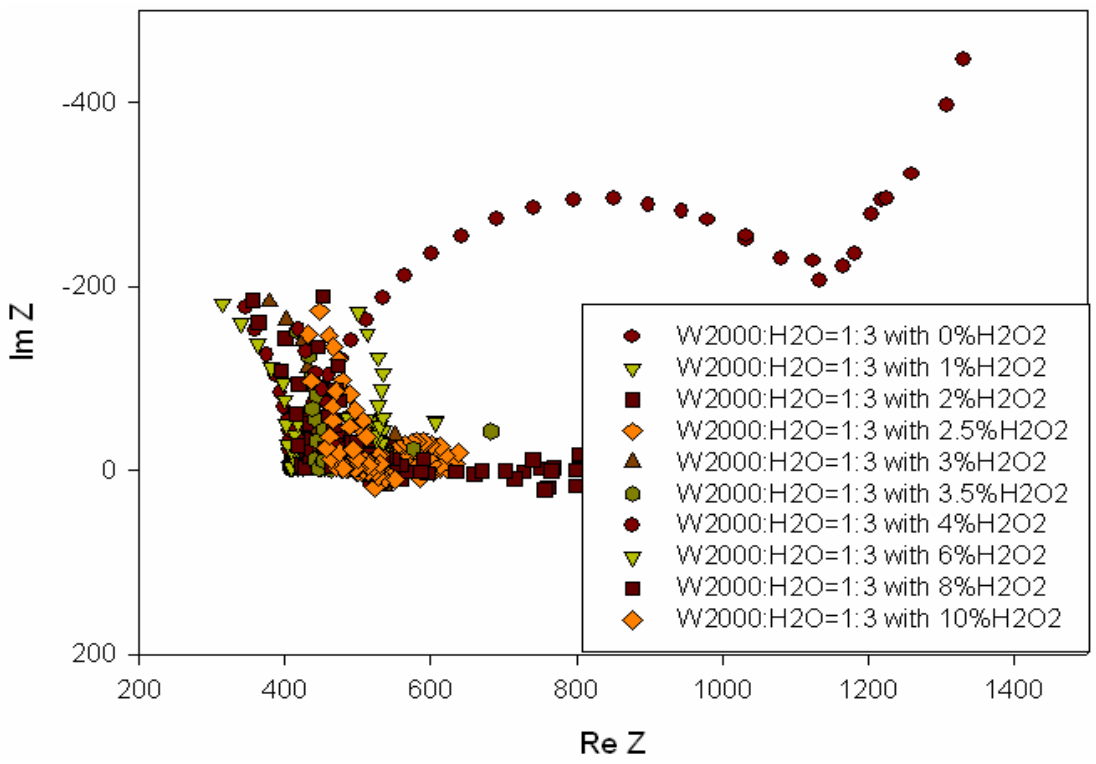

Figure 3-18 Tafel of experimental part2

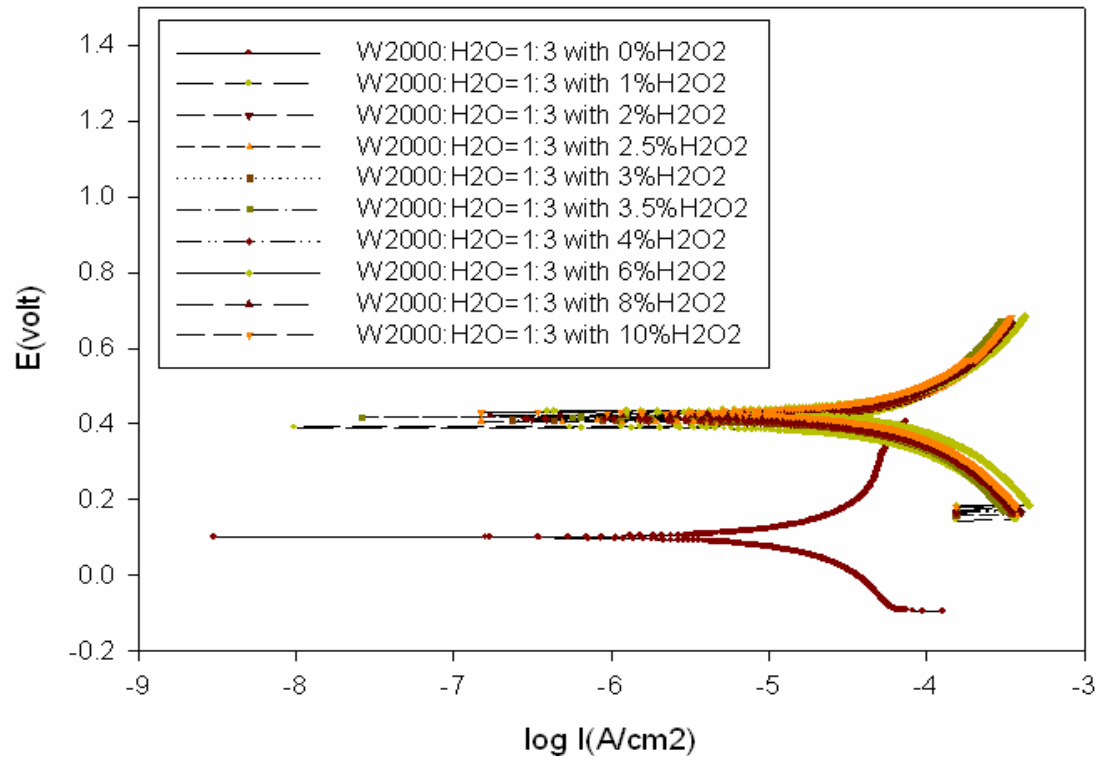

Figure 3-19 EIS of experimental part2

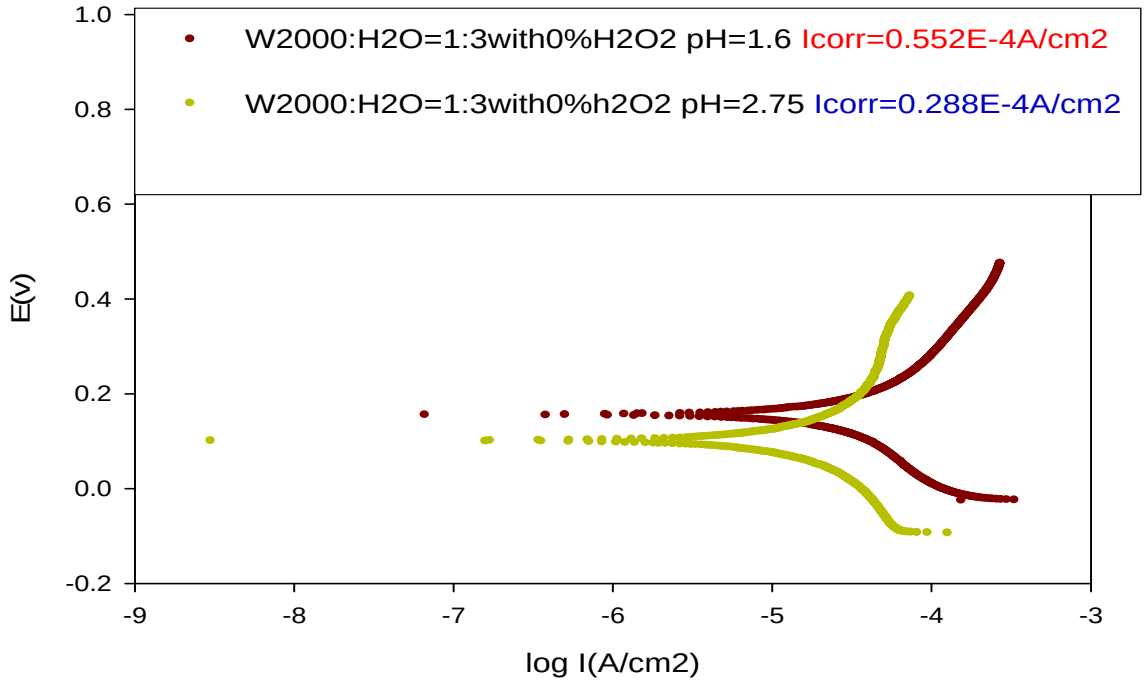

Figure 3-20 pH changing to compare corrosion current

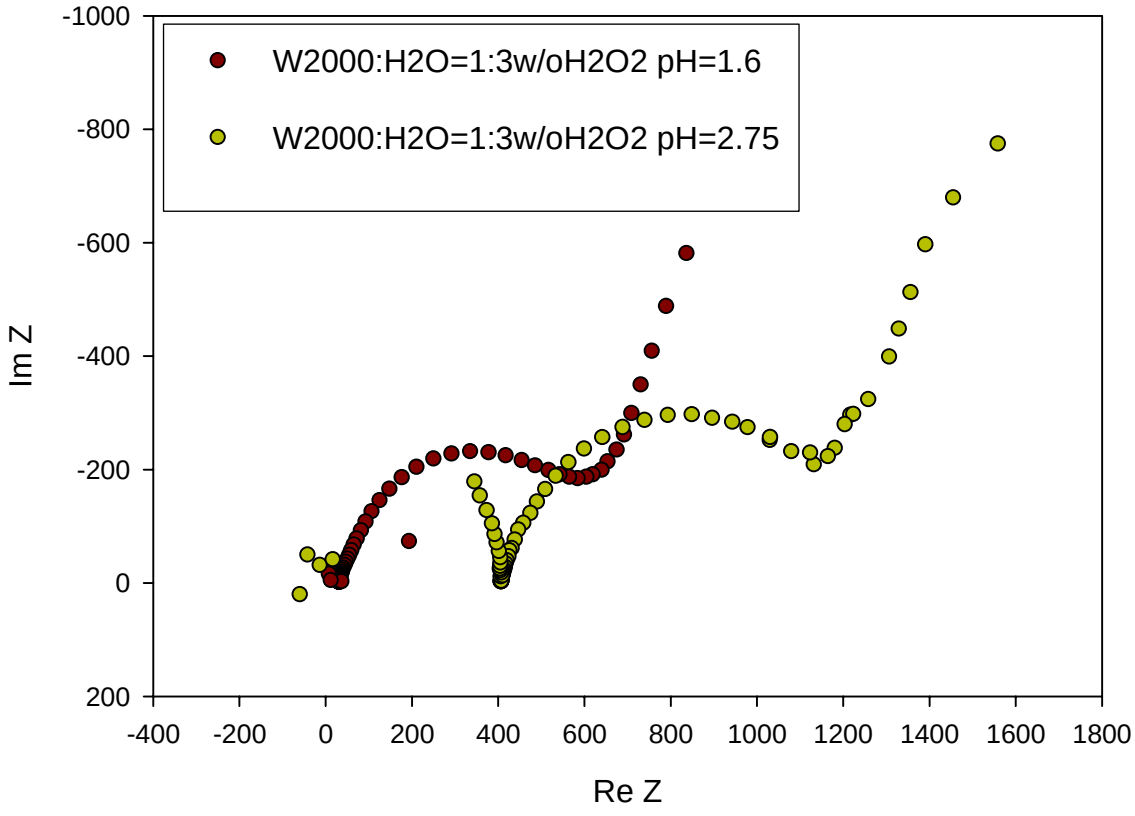

Figure 3-21 pH changing to observe EIS

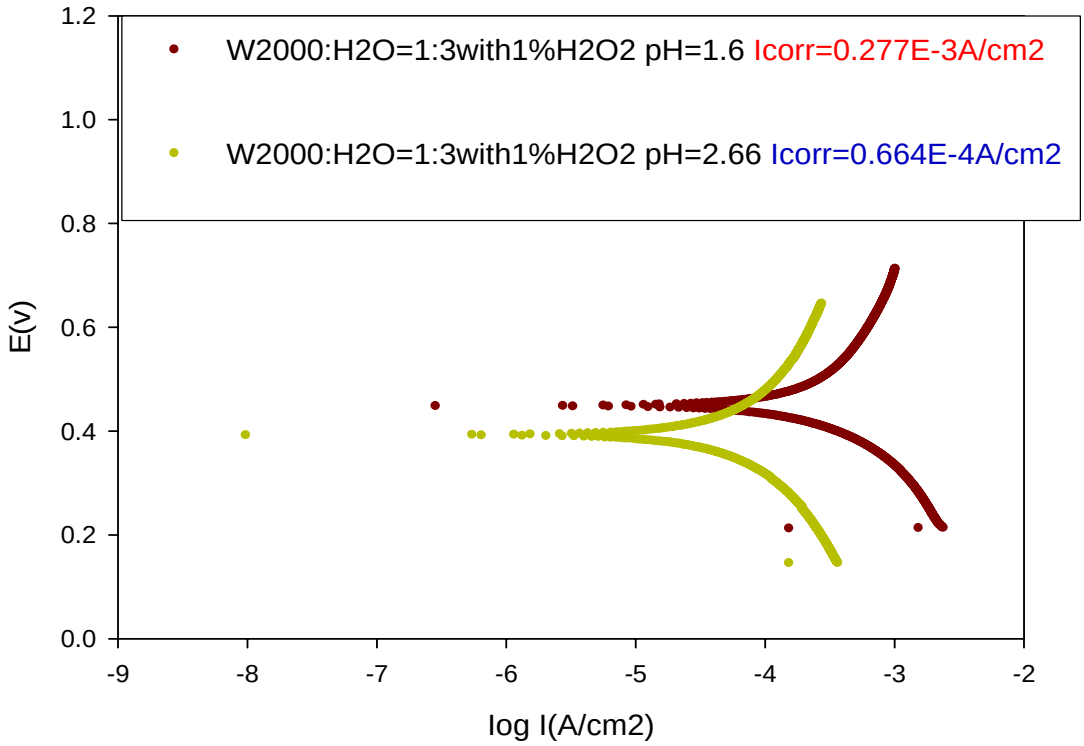

Figure 3-22 pH changing to compare corrosion current

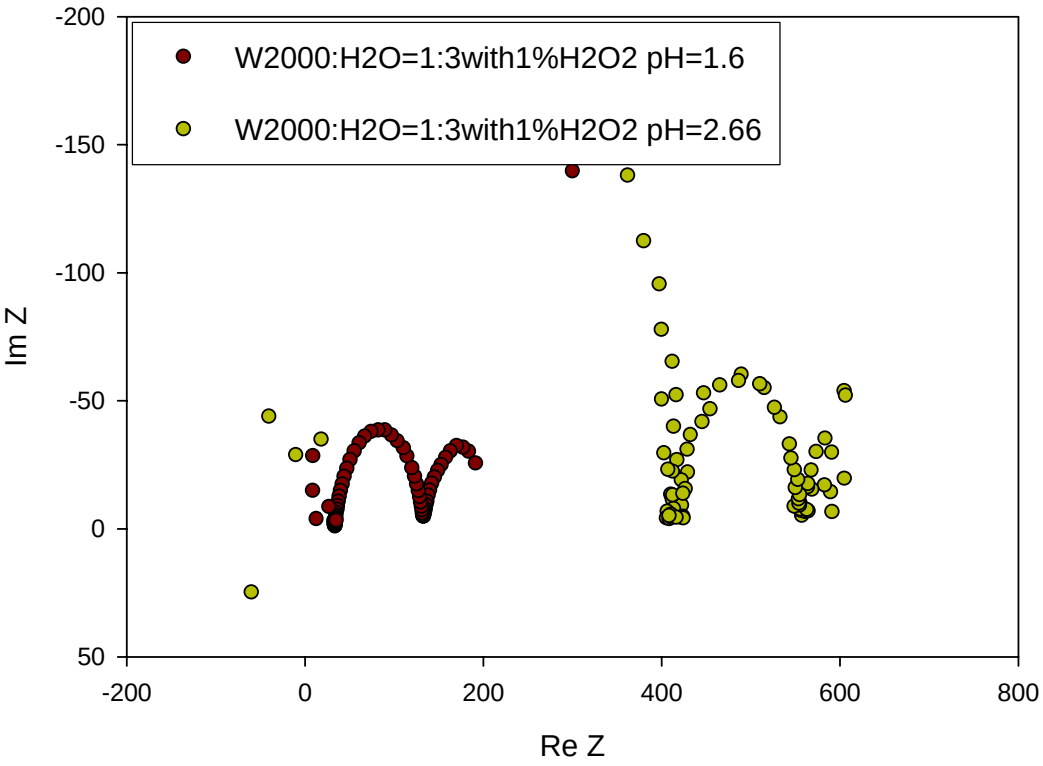

Figure 3-23 pH changing to observe EIS

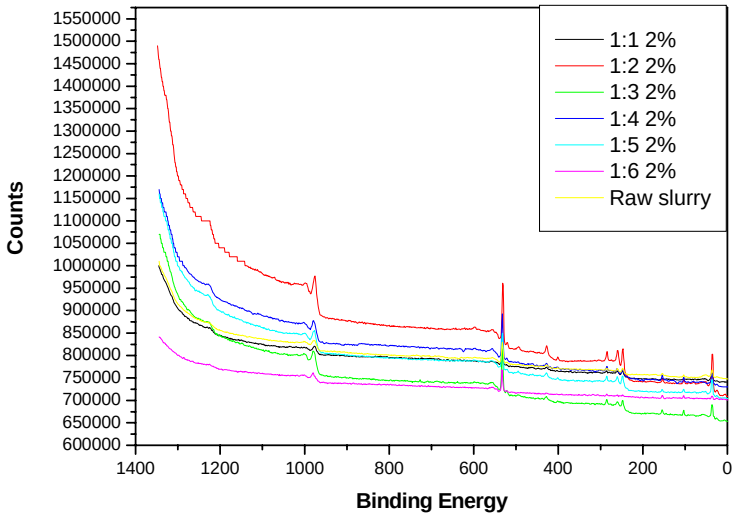

Figure 3-24 Survey of experimental part1

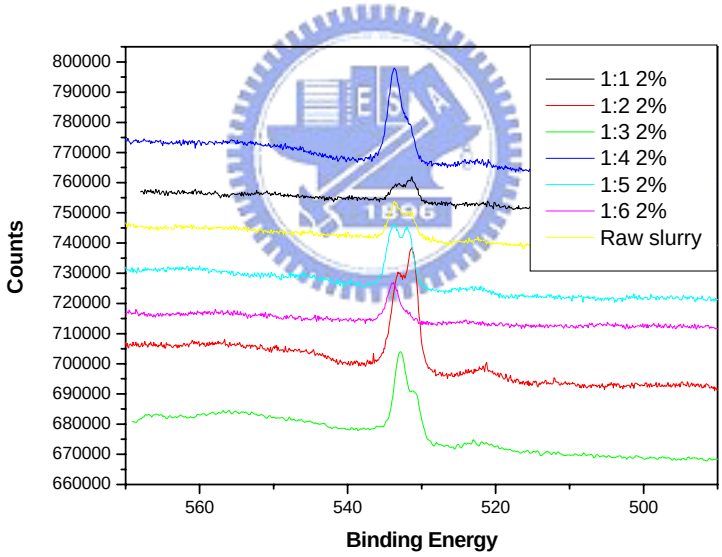

Figure 3-25 Multiplex of oxygen in the experimental part1

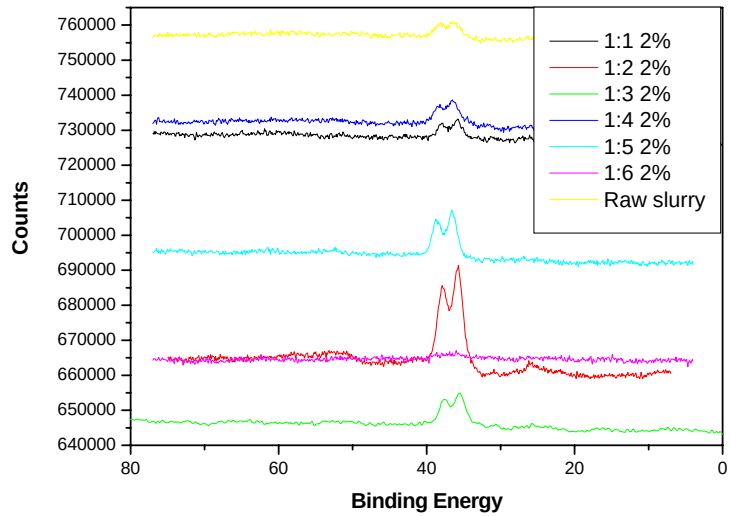

Figure 3-26 Multiplex of tungsten in the experimental part1

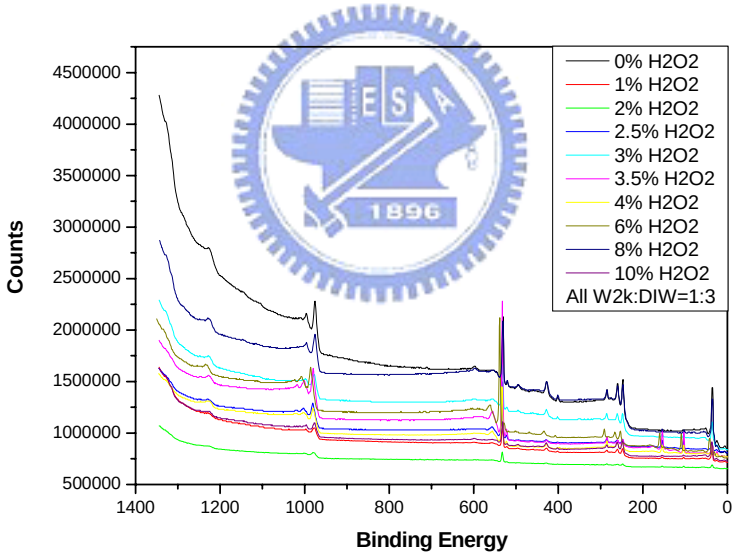

Figure 3-27 Survey of experimental part2

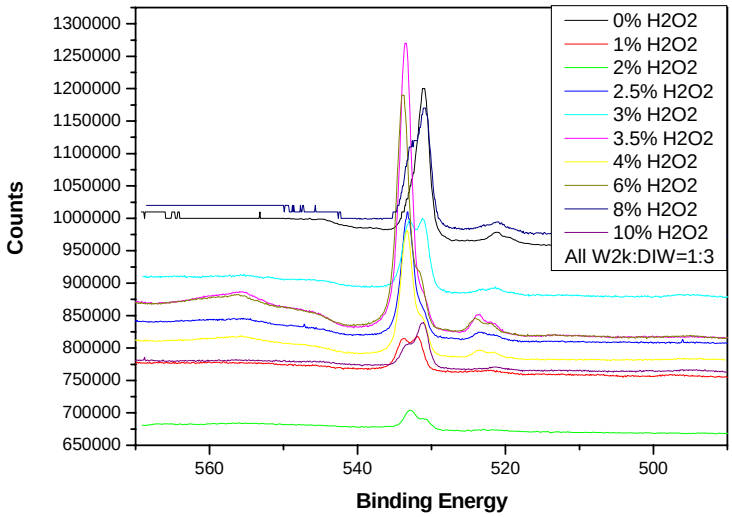

Figure 3-28 Multiplex of oxygen in the experimental part2

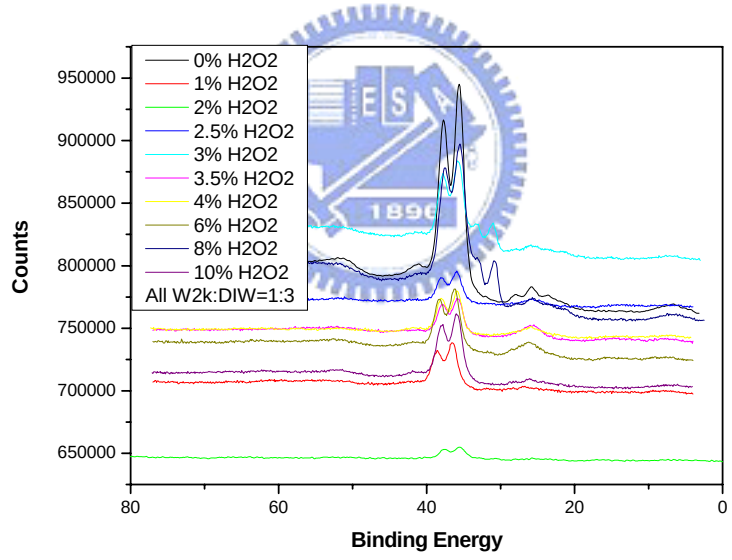

Figure 3-29 Multiplex of tungsten in the experimental part2

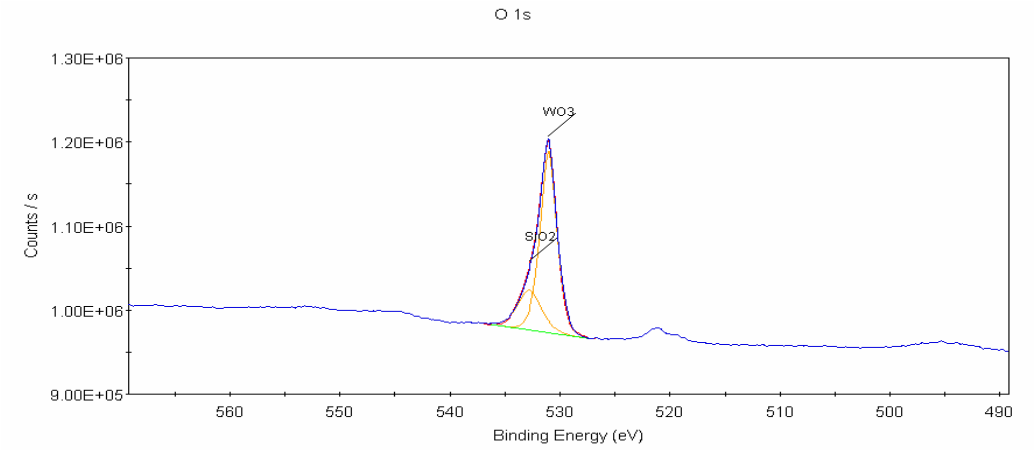

Figure 3-30 Fitting to find the WO3 around the BE of oxygen in 1:3 w/o H2O2

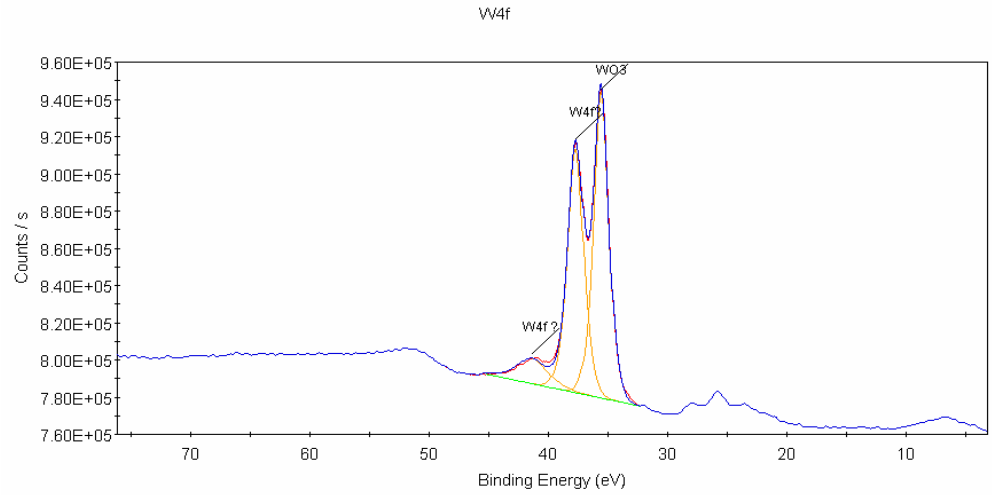

Figure 3-31 Fitting to find the WO3 around the BE of tungsten in 1:3 w/o H2O2

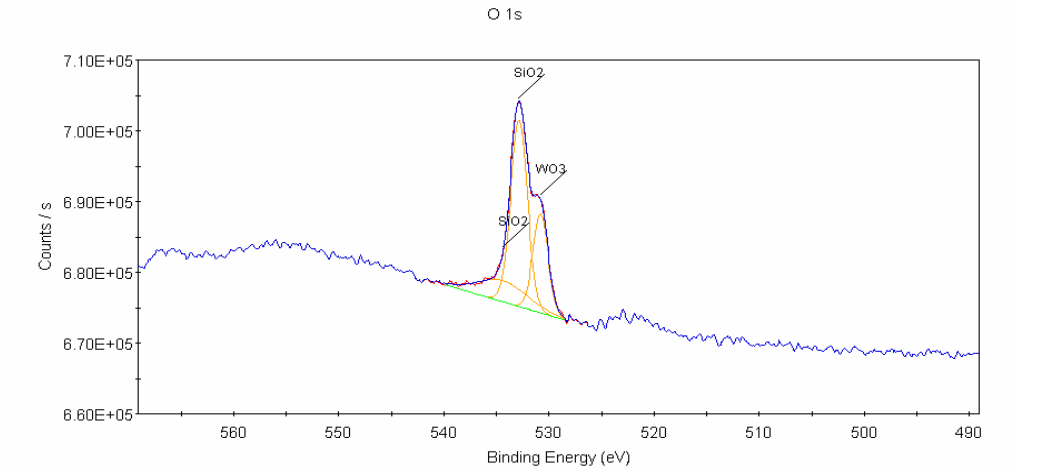

Figure 3-32 Fitting to find the WO3 around the BE of oxygen in 1:3 with 2% H2O2

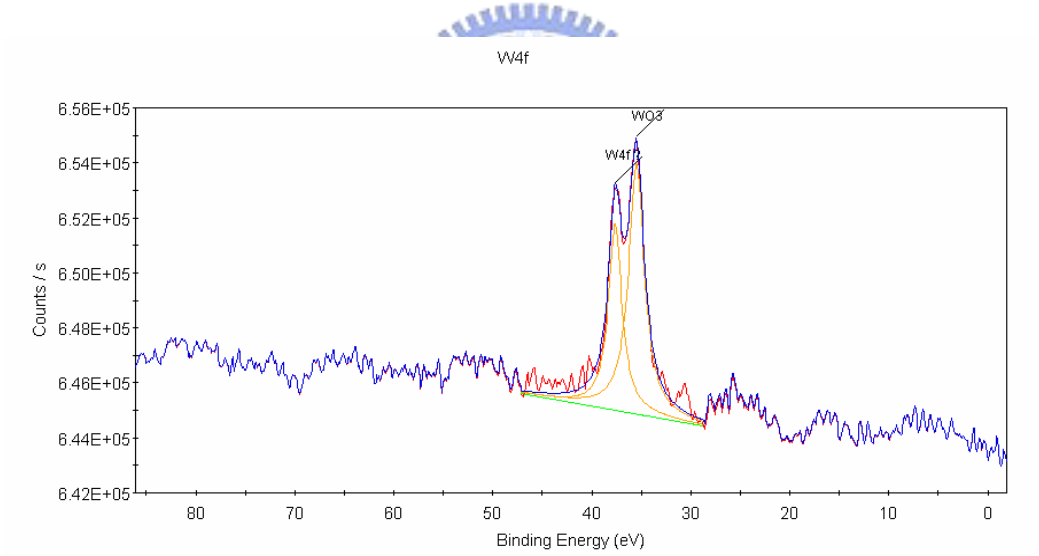

Figure 3-33 Fitting to find the WO3 around the BE of tungsten in 1:3 with 2% H2O2

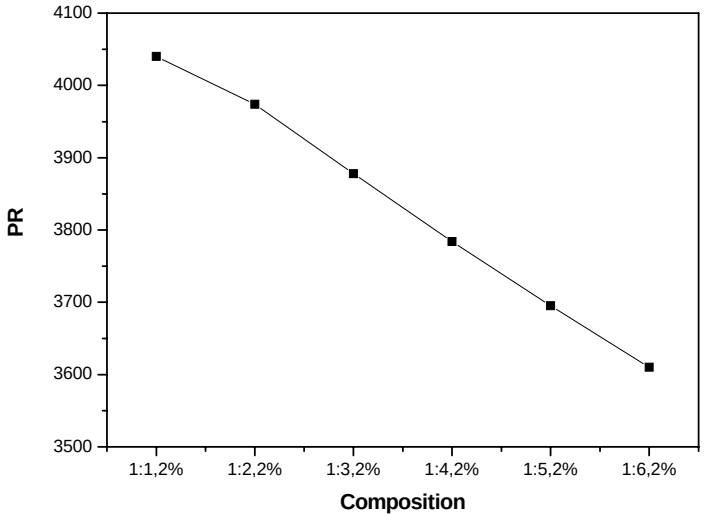

Figure 3-34 Polishing rate of experimental part1

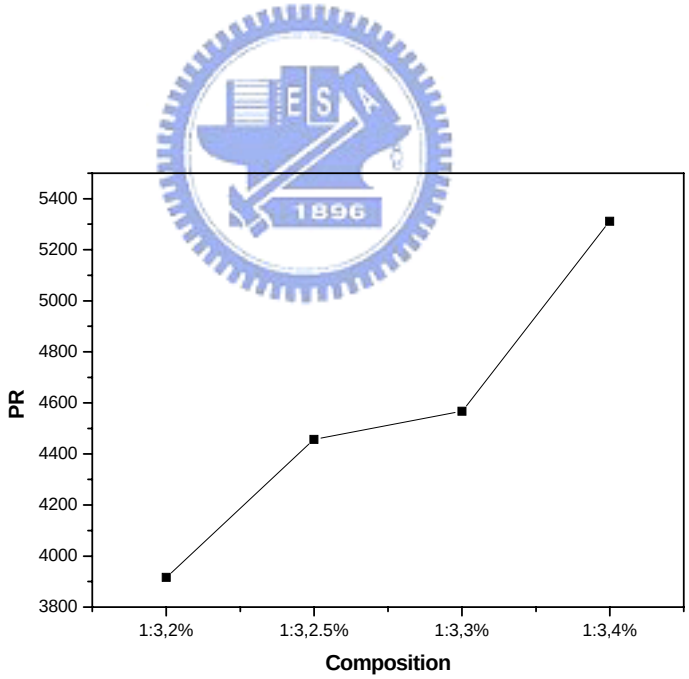

Figure 3-35 Polishing rate of experimental part2

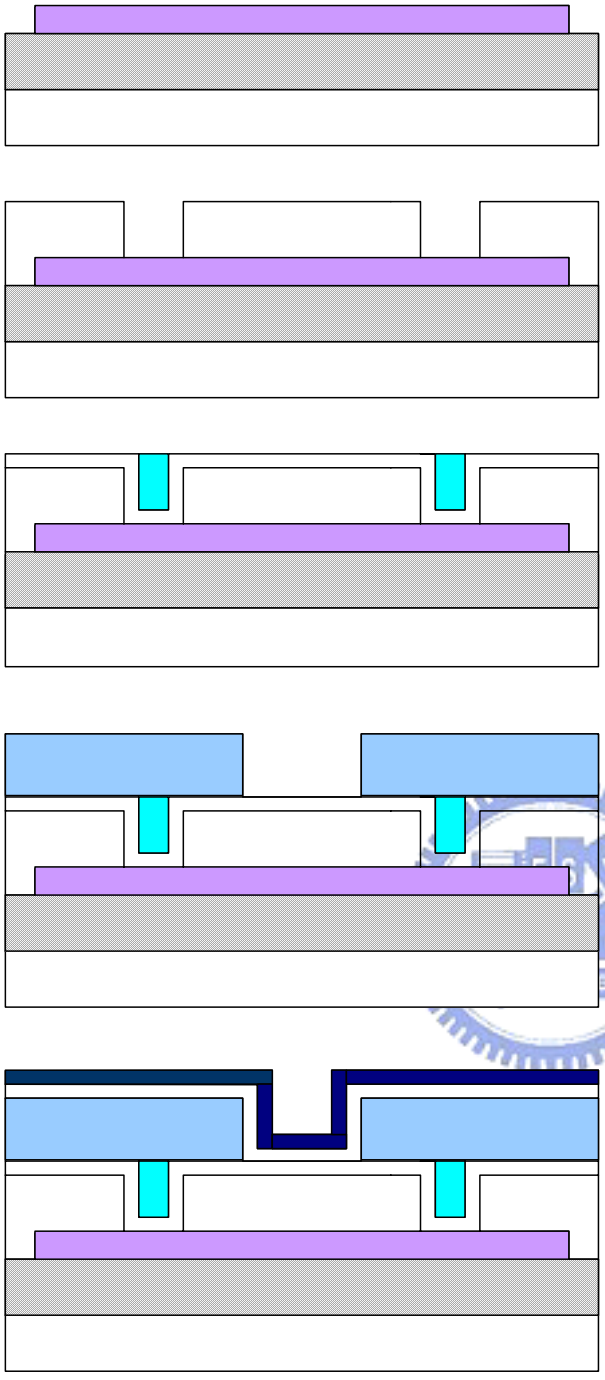

Figure 3-36 Via chain structure flow

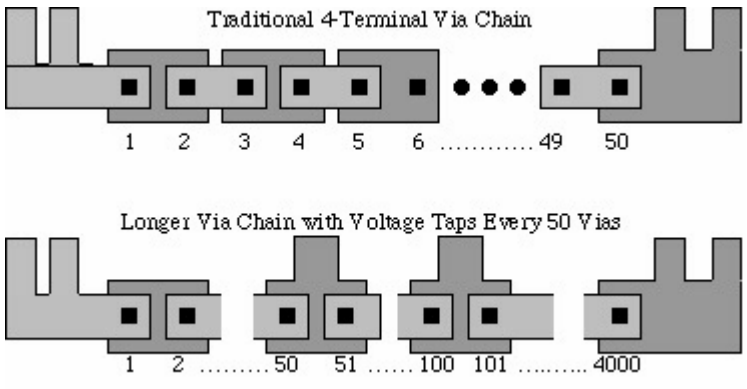

Figure 3-37 Via chain structure top view